scientific reports

Check for updates

OPEN

L-histidine in nontronite: stability under Martian-like UV irradiation to assist life detection on Mars

Cristina García-Florentino[1,5]✉, Ilaria Bergamo[1,2,5]✉, Teresa Fornaro[1], Andrew Alberini[1], Nicoletta Marinoni[2], Marco Merlini[2], Sole Biancalani[1], Francesco Renzi[1,3], Giovanni Poggiali[1], Mariano Battistuzzi[1], Elisabeth M. Hausrath[4] & John R. Brucato[1]

Detection of organic molecules on Mars is challenging due to a variety of degradation processes occurring at the Martian surface, including UV irradiation. Nevertheless, the NASA's Curiosity rover found evidence of organic molecules in clays, suggesting that these minerals might be particularly suitable to preserve organics on Mars. In this work, the photostability of L-histidine adsorbed at different pHs on nontronite under Martian-like UV irradiation was investigated in order to assess the preservation potential of this clay in the Martian environment. The interactions between L-histidine and nontronite were investigated via Infrared spectroscopy and X-Ray Diffraction, in order to understand the possible preservation mechanisms. Results indicate that L-histidine intercalates into the mineral interlayer at acidic pH, and undergoes minor degradation after UV exposure compared to the pure molecule. At basic pH, polymolecular layers are formed and no degradation is observed. These results show that nontronite acts as a photoprotective mineral for L-histidine both at acidic and basic pH, making it a suitable mineral target for organic detection on Mars.

Keywords FTIR spectroscopy, UV radiation, Molecular biosignatures, Amino acids, Mars missions

Mars has captivated scientists with its potential to have once supported life. Located at the outer edge of the Solar System's habitable zone, Mars shows evidence of past liquid water on the surface with features like ancient river and lake beds. Today, Mars has a thin, CO_2-rich atmosphere and a weak magnetic field that has contributed to the loss of much of its early atmosphere. This has left Mars with a cold, dry surface, where liquid water is no longer stable. The planet's small size and molten core with a thermal blanket that restricts heat flow have led to the cessation of the convective motions that generate the magnetic field[1,2], exposing the surface to harsh solar wind and radiation. Despite this, Mars remains a target for astrobiological research because of its already demonstrated past habitability[3–5]. The past Martian geochemical conditions were very similar to Earth where they led to the emergence of unicellular lifeforms. By analogy with Earth, it is plausible that simple microorganisms emerged also on Mars. In this context, NASA's Curiosity and Perseverance rovers, along with the future ESA's ExoMars Rosalind Franklin rover, are looking for molecular biosignatures in geological targets with the aim to uncover signs of ancient microbial life on Mars.

In the current Martian environment, however, organic compounds are very scarce as they likely undergo degradation through oxidation and photolysis/radiolysis. The effects of UV irradiation, in particular, occur quite rapidly, since many organic molecules efficiently absorb UV light and may initiate photochemical reactions in short timescales (sols to a few years)[6]. This molecular degradation time depends on the nature of the organics and the mineral matrix in which they are embedded[6]. Since UV radiation can only penetrate a few micrometres below the surface[4,6], the detection of organics is focused on the Martian subsurface. For example, the Perseverance rover uses an abrasion tool to remove the most altered surficial layer (the uppermost centimetre) to study the interior of the rocks[7]. With the same objective, the future Rosalind Franklin rover will drill down to 2 m to investigate also samples possibly not affected by Galactic Cosmic Rays (GCRs), Solar Energetic Protons (SEPs) and oxidants. Nevertheless, in both cases, after the abrasion, due to rover operation reasons, the fresh subsurface material is exposed to Martian ambient conditions for several hours until the measurement can be performed[6]. This exposure time is on the UV-induced organic photodegradation time scale, while additional effects of

[1]INAF- Astrophysical Observatory of Arcetri, L.go E. Fermi 5, 50125 Firenze, Italy. [2]Department of Earth Sciences, State University of Milan, 20133 Milan, Italy. [3]Department of Physics and Astronomy, University of Florence, Sesto Fiorentino (FI), Via Giovanni Sansone 1, 50019 Sesto Fiorentino, FI, Italy. [4]Department of Geoscience, University of Nevada, 4505 S. Maryland Pkwy, Las Vegas, NV 89154, USA. [5]These authors contributed equally to this work: Cristina García-Florentino and Ilaria Bergamo. ✉email: cristina.garcia@inaf.it; ilariabergamo29@gmail.com

GCRs and SEPs are expected to occur on a much longer timescale[4]. Considering this factor, it is fundamental to investigate the stability of organics embedded into possible Martian mineral matrices under Martian-like UV radiation to understand the actual detectability of possible molecular biosignatures with rover payload instruments[8].

Even though the occurrence of organic molecules on Mars is rare, the Perseverance rover has already detected some organics on Mars; specifically polycyclic aromatic hydrocarbons within sulfates precipitated in the pores of igneous rocks in the Jezero crater[9], and macromolecular organic carbon of possible biotic origin within a mudstone deposited in the main inlet channel into Jezero crater[10]. On the other hand, the Curiosity rover has also detected a variety of organic molecules, such as sulfur- and chlorine-bearing aliphatic and aromatic organic compounds, carboxylic acids, polycyclic aromatic hydrocarbons[11,12] and long-chain alkanes up to 12 carbon atoms[13] in lacustrine mudstone sediments at Gale crater. This association with mudstones rich in smectite clay minerals suggests that clays may efficiently preserve organics in the harsh Martian environment.

In this work, the photostability of the amino acid L-histidine adsorbed onto the clay mineral nontronite at acidic and basic pHs under Martian-like UV irradiation was studied. The aim of the work is to understand if this kind of molecular biosignature of extant life might resist in the Martian environment long enough to be detected once revealed by the rovers from the subsurface. Considering the smectite clay rich environment of Gale crater where many organics were identified and the identification of nontronite in multiple locations on Mars, nontronite was selected as the mineral matrix[14–16]. On the other hand, the L-histidine amino acid was selected as a possible target for life detection as an organic molecule biotically relevant for life as we know it and because of its different possible pH-dependent protonation states that may affect the kind of bonding with the mineral. In fact, the adsorption of the amino acid was performed at different pHs to study the adsorption into the interlayer regions or the external surfaces of the clay mineral, potentially affecting its photostability under Martian-like UV irradiation[17,18].

The characterization of L-histidine into nontronite pre- and post-irradiation has been carried out by means of Infrared spectroscopy (IR) and X-Ray diffraction (XRD) techniques. Infrared spectroscopy provides information on molecule-mineral interactions, which in turn may affect molecular photostability, and produces datasets comparable to the mission data acquired by instruments such as SuperCam on Perseverance[19–21], Micromega[22] and Ma_MISS[23] on ExoMars, which employ Near Infrared (NIR) vibrational spectroscopy. X-ray Diffraction provides insights into the changes of the structure of the mineral as a consequence of molecular adsorption, which is key to inspect the possible preservation mechanisms.

Results

X-ray diffraction characterization

Figure 1 shows the X-ray diffraction patterns of the analysed samples corresponding to nontronite diffraction peaks, no XRD peaks were attributable to crystalline L-histidine. The pure sample of untreated nontronite is indicated in blue, and exhibits the characteristic reflection at 3° 2θ (≈ 13 Å), corresponding to the basal plane *(001)*. This is accompanied by a series of *hkl* broadened diffractions bands indicative of turbostratic layer stacking, that is without orderly stacking arrangements[24]. The samples treated at acidic pH, without and with L-histidine, are represented in black and green, respectively, and exhibit peaks attributable to halite (NaCl).

Despite molecular adsorption, the fundamental nontronite structure is still preserved: all *(00 L)* and *hkl* peaks remain sharp, with the only systematic change being a shift of the basal reflections toward higher *d* values. This is particularly evident in the inset of Fig. 1, where the position of the *(001)* peak and the *hkl*-band is compared for

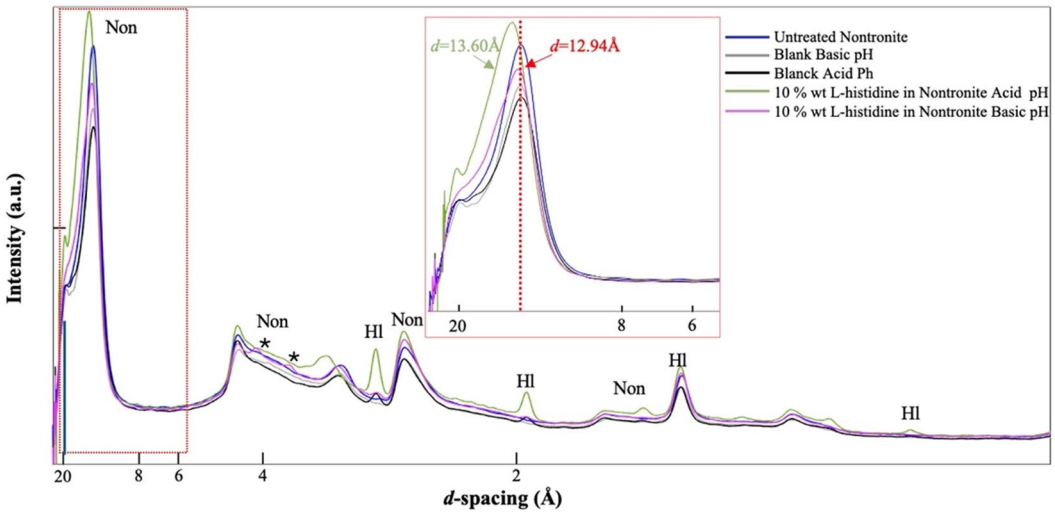

Fig. 1. XRD patterns of all samples. Inset: Shifts toward higher d values in the peaks of the 10wt.% L-histidine in nontronite at acidic pH (green) compared to the other samples. Symbol: Hl: halite; Non: nontronite. * Traces of sodium sulfate thenardite from nontronite synthesis. XRPD patterns acquired using Mo X-Ray source.

untreated nontronite and the sample with L-histidine adsorbed on nontronite at acidic pH. Such displacement corresponds to an increased interlayer spacing, thus reflecting a change in the hydration state or incorporation of additional molecules, as L-histidine, in the interlayer region. In addition, Fig. 1 shows a slight shift in the basal reflection peak for 10% L-histidine in nontronite at basic pH. This shift resulting in an increase in d-spacing cannot be attributed to the adsorption of L-histidine, because in that case, a much larger shift, comparable to the one observed for the L-histidine adsorbed at acidic pH would be expected. In this case, this difference observed for the basic pH may be related to the incorporation of OH^- groups or Na^+ ions within the interlayer due to the basic treatment.

Finally, peak-profile analysis of high-resolution data yields coherent domain sizes of ~10 nm for every sample. The uniformity of these values indicates that the presence of the molecule does not appreciably affect the crystallinity or domain dimensions of the nontronite phase.

Infrared characterization

After the adsorption of the molecule onto the mineral, in the NIR/MIR infrared spectral range (8000–400 cm^{-1}), some vibrational bands of pure L-histidine can still be observed when adsorbed onto nontronite at 10 wt% at both acidic (4.6) and basic (9.8) pHs, although most of the L-histidine bands disappear when adsorbed on nontronite (Table 1 and Figure S1 and S2 from Supplementary Material). This likely due to the broad bands of the mineral

Pure L-histidine (cm^{-1})	L-histidine in nontronite Acidic pH (cm^{-1})	L-histidine in nontronite Basic pH (cm^{-1})	Vibrational mode assignment
6164/6141	6204 (+40)	6160 (−4)	-
5871	-	5863 (−8)	-
5819	5817 (−2)	5823 (+4)	-
5668	-	5659 (−9)	-
4627	4587 (−40)	4623 (−4)	-
4442	-	4442 (0)	-
4378	-	4374 (−4)	-
4297	-	4295 (−2)	-
4212	4218 (+6)	4212 (0)	-
4102	-	4102 (0)	-
4058	-	4054 (−4)	-
2349	-	2344 (−5)	-
2309	-	2309 (0)	-
2284	-	2284 (0)	-
2214	-	2220 (+6)	-
2152	-	2150 (−2)	-
1792	1776 (−16)	1784 (−8)	C = O ν. +NH δ[26]
1661	-	1629 (−32)	asymmetric COO ν + NH δ[26]
1597	1610 (13)	1595 (−2)	asymetric NH δ[27]
1575	-	1570 (−5)	-
1506/ 1489 (shoulder)	1501 (−5)	1495 (−11)/1468shoulder	NH in plane δ[27], NH in plane δ and C = N ν[28]
1429	1431 (+2)	1431 (+2)	CH_2 δ[28,29]
1406	1416 (+10)	1421 (+15)	COO^- ν[28,29]
1350/1335	1338 (−12)	1348 (−2)	δ NH_3^+[2830,]/δ out of plane CH_2 (wagging)[28,29,31]; CH_2 δ[28]
1317	1312 (−5)	1315 (−2)	CH_2 δ, =CH δ[28]
1273	1286 (+13)	1271 (−2)	CH δ, =CN ν[28]
1258	1261 (+16)	1254 (−4)	CH_2+ NH_3^+δ[26]
1223	-	1221 (−2)	-
1150	-	1153 (+3)	NH_2 twist + CH δ + CN ν CN ν[27]
1111	-	1115 (+4)	-
1088	-	1088 (0)	-
1061	-	1068 (+7)	mixed vibration of NH_3^+ CH δ[26]
852	868 (+16)	852 (0)	mixed vibration of NH_3^+CH δ[27]

Table 1. Infrared bands of pure L-histidine and adsorbed onto nontronite at acidic and basic pHs with the vibrational mode assignment and vibrational shifts with respect to the pure L-histidine reported in parenthesis. In grey, molecular bands detectable in the adsorbed sample but not integrated because obscured by the mineral bands or too weak to be integrated. **ν** = stretching; **δ** = bending; between brackets: vibrational shifts respect to the pure molecule.

partially masking the one belonging to the molecule. The bands of nontronite and their corresponding suggested assignments based on the work by Frost et al.[25] can be checked in Table S1 from Supplementary Material. In addition, some of the L-histidine bands that can still be appreciated when the molecule is adsorbed are shifted with respect to the ones in the pure molecule. These shifts ($>4\ cm^{-1}$) observed for some IR bands of the molecule may be indicative of possible interactions between the mineral and the functional groups of the molecule. Different protonation states of the molecule can cause also a shift of the bands however, after recrystallization, different protonation states from the expected zwitterionic state of the molecule can only be expected due to molecule-mineral interactions. If there is no interaction between a basic or acidic ionic functional group of the molecule and the mineral in solution, after the recrystallization, the reprecipitation of pure L-histidine in its normal solid zwitterionic (H_3N^+-CHR-COO^-) would be expected causing no shifts with respect to pure L-histidine. Therefore, the observed shifts on the new precipitates can only be due to an interaction between the different protonation states of the basic or acidic forms of L-histidine and the mineral. This fact may cause a shift due to the different protonation states of the molecule only possible on the new solid due to the interaction with the mineral or due to the interactions with the mineral itself. These interactions, such as electrostatic interactions or other weaker adsorption forces like van der Waals in the case of a physical adsorption, may also change the bond strength of the functional groups. In this case, after both absorption processes, it can be observed that the amino and carbonyl groups exhibit the greatest shifts (see Table 1).

Degradation induced by UV-radiation

In Fig. 2, an example of the degradation induced by UV radiation of the L-histidine bands in the range 1500–1000 $cm^{-1}$is shown. In this Fig. 2, all acquired spectra at different irradiation times are shown for pure L-histidine and L-histidine adsorbed at different pHs. A zoom for the band at 1429 cm^{-1} is shown as an example, where the change of the band can be appreciated along the irradiation time together with the corresponding baseline corrected and flipped band for integration. The areas employed for plotting the degradation curves were integrated from these baseline corrected bands shown in Fig. 2C.

In the region of the IR spectra > 4000 cm^{-1} corresponding to the non-fundamental vibrational modes, among the L-histidine bands that can still be detected after the adsorption onto nontronite, some bands can be analysed both in acidic and basic adsorptions after UV irradiation (see Table 1 and Figures S1A and S2A in Supplementary Material). The bands at 6164 and 6141 cm^{-1} of the pure molecule, when adsorbed onto the mineral, merge to

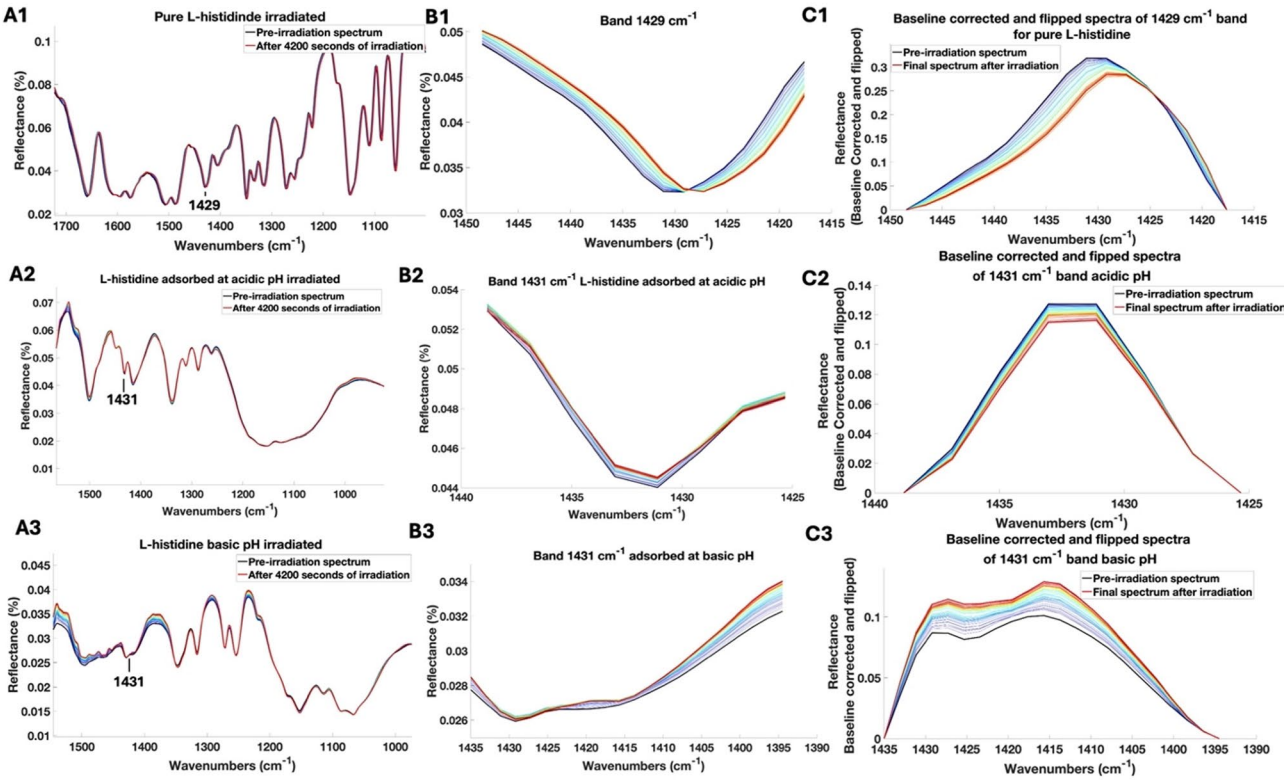

Fig. 2. (**A**) Spectral ranges containing most of the bands of L-histidine for all the acquired spectra during the irradiation steps being. Black spectrum acquired at t0s of irradiation (after 40 min N_2 pumped) and the red spectrum acquired at t4200s for A1) pure L-histidine, A2) L-histidine adsorbed at acidic pH and A3) L-histidine adsorbed at basic pH. (**B**) Zoom of the example band at 1429 cm^{-1} A1) pure L-histidine, A2) L-histidine adsorbed at acidic pH and A3) L-histidine adsorbed at basic pH. (**C**) Baseline corrected and flipped zoom of the example band at 1429 cm^{-1} showing the final integrated areas for C1) pure L-histidine, C2) L-histidine adsorbed at acidic pH and C3) L-histidine adsorbed at basic pH.

form a single band both in basic and acidic conditions. None of these bands show any degradation after the irradiation when the molecule is adsorbed on the mineral, while both bands degrade in the pure L-histidine as can be observed in *S3 from Supplementary Material*. The bands of the molecule that fall within the range of 5880–5650 cm^{-1}, in the acidic adsorption, appear as a single very weak and broad band (see Figure S1A from Supplementary Material) that does not degrade after the irradiation experiments. In the basic adsorption conditions, they remain separate, very weak (Figure S2A), and they still do not show any sign of degradation after the UV irradiation experiments. The L-histidine bands in the range 4000–5000 cm^{-1} cannot be observed in the sample adsorbed at acidic pH with the exception of the band at 4212 cm^{-1} (See Figure S1A) while there are few more visible in the basic adsorption (4442, 4374, 4295, 4212, 4102, 4058 cm^{-1} respectively) (see Figure S2A from Supplementary Material). However, these bands with the only exception of the band at 4212 cm^{-1} are very weak and overlap with the mineral bands, so they have not been considered in the degradation kinetics analysis to avoid misinterpretations. The bands at 4627 and 4212 cm^{-1} of the pure molecule can instead be integrated for both samples adsorbed at acidic and basic pH. As shown in Figure S3, the fastest degradation occurs for pure L-histidine compared to the ones adsorbed at acidic pH, where the process is slower, and in the basic where there is no evidence of degradation for any of the bands (Figure S3). The calculated Martian half-life times and degradation cross sections of the bands are summarized in Table 2.

In the region between 4000 and 1600 cm^{-1}, some weak bands of the pure molecule are detectable, and can also be observed in the samples adsorbed onto nontronite at both pHs. However, these bands have not been considered in the degradation kinetics analysis due to their overlap with the mineral bands or due to their low intensity (Figure S1a and S1b). Between 2350–2100 cm^{-1} some weak bands can be observed specially in the case of L-histidine adsorbed at basic pH (See Figures S1B and S2B) but none of these bands have been considered for the degradation studies due to their low intensity and overlap with mineral bands.

Most of the bands of L-histidine adsorbed onto nontronite can be detected on the range 1800 to 1200 cm^{-1} (Figure S1C and S2C). However, caution must be taken when integrating the bands in the range 1880 and 1300 cm^{-1} because the bands of residual atmospheric water are also present (See this effect specially in Fig. 2A3 for >1500 cm^{-1}). Residual atmospheric water may cause some changes in the bands at the beginning of the irradiation. If the band is too weak or the change in the band due to the degradation is too small, the degradation of the bands due to the UV radiation may be affected by very small change in the atmospheric water. This may create an initial increase in the fitted degradation trend which tends to be stabilized as time passes and nitrogen is pumped. Before initiating the experiments, nitrogen was pumped for 40 min, but sometimes this time is not enough to stabilize the atmospheric water in the sample chamber. An example of this can be observed in the degradation curves of the bands 1506 and 1489 cm^{-1} in the pure molecule that combine in one band both in the acidic (main peak at 1501 cm^{-1}, with 1481 cm^{-1} shoulder) and the basic (main peak at 1495 cm^{-1} with 1468 cm^{-1} shoulder) samples (See Figure S4). In the pure molecule and in the sample adsorbed at acidic pH, the changes observed for the band during the irradiation time start with an increase in the area due to the decrease of atmospheric H_2O as N_2 is pumped in the sample chamber (Figure S4). The half-life times for these bands have not been calculated as the fitting to the experimental data cannot be obtained due to the initial increase of the

	Martian $t_{1/2}$ (h)			σ (cm^2) ($\cdot 10^{-21}$)		
Wavenumbers (cm^{-1}) Pure | acid | basic	**Pure L-histidine**	**10 wt% L-histidine acid pH**	**10 wt% L-histidine basic pH**	**Pure L-histidine**	**10 wt% L-histidine acid pH**	**10 wt% L-histidine basic pH**
6164 – 6141 | 6204 | 6160	20 ± 2	Spr. data S.B.	Spr. data S.B.	6.9 ± 0.8	Spr. data S.B.	Spr. data S.B.
5871-5819-5765 | 5817 | X	22 ± 3	Spr. data S.B.	X	6.3 ± 0.8	Spr. data S.B.	X
5871 | X | 5863	21 ± 3	X	Spr. data S.B.	6.6 ± 0.8	X	Spr. data S.B.
5819 |X| 5823	26 ± 4	X	Spr. data S.B.	5.2 ± 0.8	X	Spr. data S.B.
5668 | X | 5659	23 ± 3	X	Spr. data S.B.	5.2 ± 0.8	X	Spr. data S.B.
4627 | 4587 | 4623	15 ± 2	28 ± 7	Incr. Bck and Spr.data	8.8 ± 0.8	5 ± 1	Incr. Bck and Spr.data
4212 | 4218 | 4212	25 ± 3	70 ± 20	Spr. data S.B.	5.5 ± 0.7	2.5 ± 0.7	Spr. data S.B.
1506 and 1489 sh| 1501 (1481 sh) | 1495 (1468 sh)	Init. incr. Trend due to Atm. Water	Init. incr. Trend due to Atm. Water	Atm. Water	Init. incr. Trend due to Atm. Water	Init. incr. Trend due to Atm. Water	Atm. Water
1429 | 1431 | 1431	23 ± 3	40 ± 4	Atm. water	6.1 ± 0.8	3.4 ± 0.3	Atm. water
1406 | 1416 | 1421	17 ± 2	40 ± 4	Atm. water	8 ± 1	3.4 ± 0.4	Atm. water
1350 – 1335 | 1338 | 1348	19 ± 2	26 ± 3	Atm. water	7.4 ± 0.7	5.2 ± 0.5	Atm. water
1317 | 1312 | 1315	14 ± 1	58 ± 9	Atm. water	10 ± 1	2.4 ± 0.4	Atm. water
1273 | 1286 | 1271	20 ± 1	36 ± 4	Atm. water	10 ± 1	3.8 ± 0.4	Atm. water
1258 | 1261 | 1254	23 ± 3	200 ± 100 S.B.	Atm. water	6.0 ± 0.8	0.9 ± 0.6	Atm. water
966 | X | 962	20 ± 2	X	Spr. data S.B.	6.9 ± 0.8	X	Spr. data S.B.
852 | 868 | 852	14 ± 2	S.B.	S.B.	9 ± 1	S.B.	S.B.

Table 2. Degradation cross sections (**σ**) and comparison of the Martian half-life times ($\mathbf{t_{1/2}}$) for the pure L-histidine and the L-histidine adsorbed on nontronite at pH 4.6 and 9.8. Atm. Water: Band affected by small changes in atmospheric water; Incr.Bck: Increasing tendency due to variations in the background; Spr. data S.B.: Spread data due to low intensity band; S.B: Band too small to be integrated.

signal due to the atmospheric water change. However, as it can be observed in Figure S4, once the atmospheric water is stabilized around 500 s, pure L-histidine and the L-histidine adsorbed at acidic pH start to degrade due to the UV radiation while the sample adsorbed at basic pH remains constant (Figure S4). Notice also that, when L-histidine is adsorbed at acidic pH, the degradation is slower than the one observed for the pure molecule (as shown by comparison of the slopes of the degradation curves in Figure S4).

The following bands 1429, 1406, 1350 and 1335, 1317, 1273, and 1258 cm^{-1} of the molecule (Figs. 3, 4A and 5), after the irradiation, show a greater degradation in the pure with much shorter half-lifetimes compared to the respective ones for the sample adsorbed at acidic pH (1431, 1416, 1338, 1312, 1286, 1261 cm^{-1}) and do not show any sign of degradation in the sample adsorbed at basic pH (1431, 1421, 1348, 1315, 1271, 1254 cm^{-1}) (see Figs. 2, 3, 4A and 5 *and* Table 2). As there is an increase in the samples adsorbed at basic pH due to background effects, the kinetic parameters of pure L-histidine and L-histidine adsorbed at acidic pH may be somewhat underestimated. For the bands at 1429 and 1317 cm^{-1}, the degradation curves arrive to a slightly lower At/At0 values for L-histidine adsorbed at acidic pH respect to pure L-histidine (see Fig. 5). This is likely due to a specific slightly higher degradation of the specific chemical bonds related to those specific bands, which are related to CH_2 groups. However, this is not a general trend for the rest of the bands where the pure molecule is also highly degraded (degradation curves for pure molecule arriving to the plateau at lower At/At0) (see Figs. 3 and 4 and figure S3 and S4). Anyway, the speed of degradation of these two bands related to the CH2 group is still faster for pure L-histidine than for L-histidine adsorbed at acidic pH and therefore the degradation half-life times for pure L-histidine are still much shorter also for this functional group (see Table 2).

Between 1225 and 1060 cm^{-1} *(Figure S1b*, Table 1), no bands of L-histidine can be observed in the adsorbed sample at acidic pH, while some weak bands can be observed in the one at basic pH. These range is masked by the broad band of nontronite corresponding to the Si-O stretching[25] making it impossible to observe any of the bands when the molecule is adsorbed at acidic pH. The small bands appearing inside this mineral band at basic

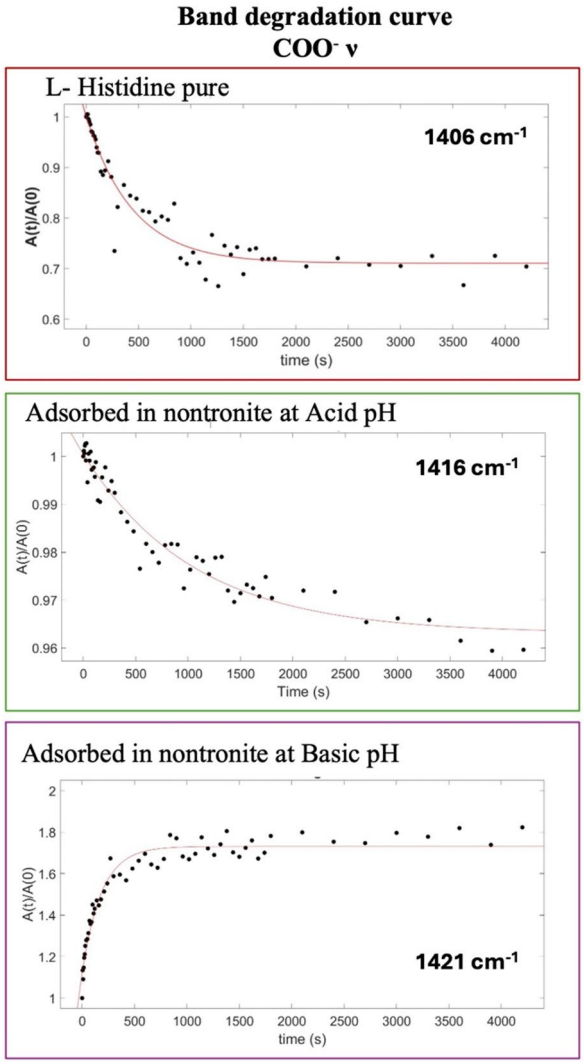

Fig. 3. Degradation curves for one of the bands assigned to the carboxylate functional group.

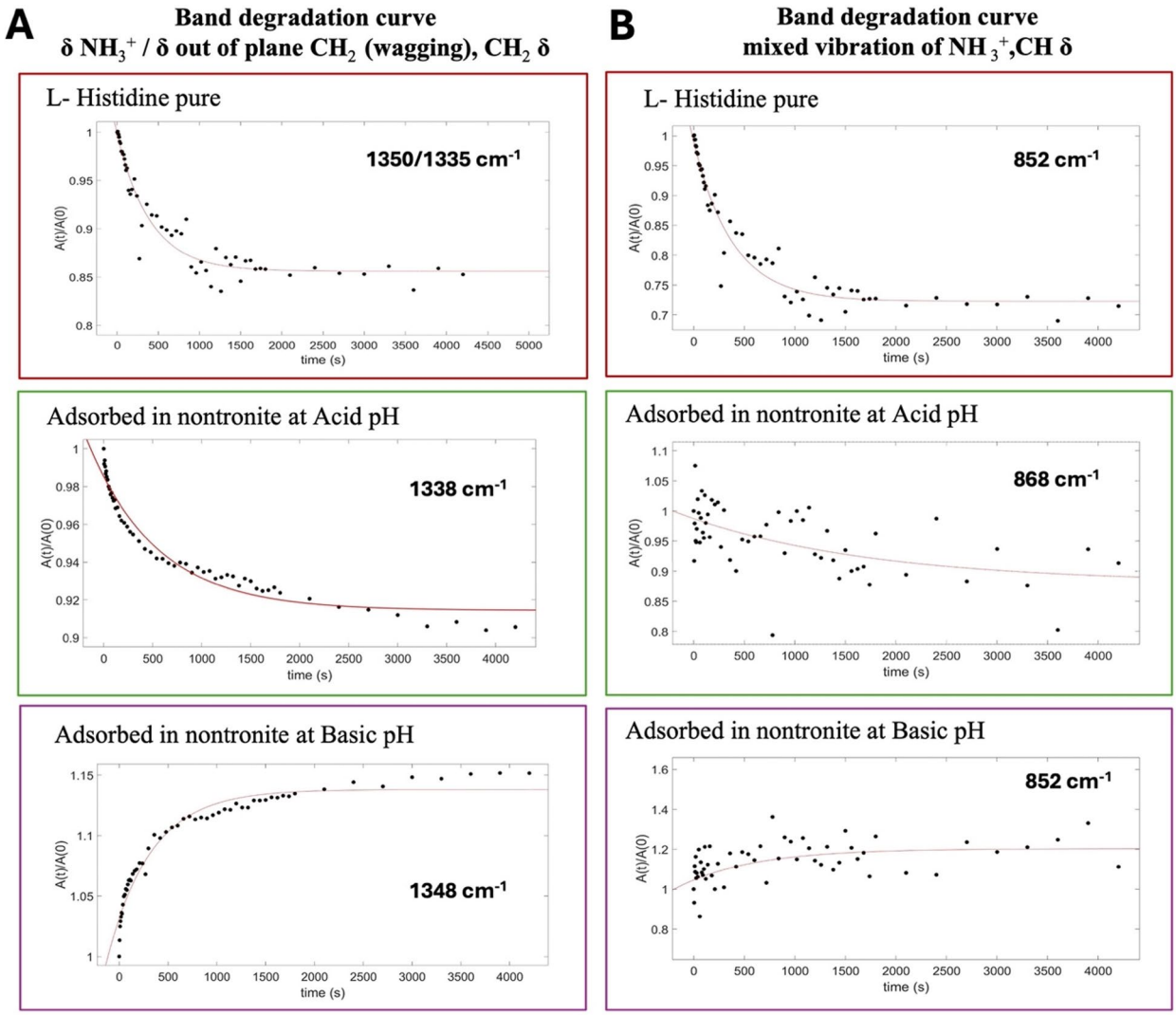

Fig. 4. Degradation curves for some of the bands partially related to the amino functional group.

pH have not been used in the degradation kinetics analysis because they are also obscured by the absorption of the mineral.

In the low wavenumber IR range, the band at 966 cm^{-1} in the pure molecule is not present in the sample adsorbed at acidic pH while it is very weak in the one adsorbed at basic pH and does not show any sign of degradation. The band at 852 cm^{-1} of the pure molecule shows a faster degradation, than the one observed for the sample adsorbed at acidic pH (868 cm^{-1}), while no degradation is observed for the one adsorbed at basic pH (852 cm^{-1}) (See Fig. 4B). As it can be observed for this band when the L-histidine is adsorbed at basic pH, the background effects on this lower wavenumber part of the spectrum are smaller. However, the bands observed in when L-histidine is adsorbed are weak and the errors in the degradation times are high. Therefore the half-lifetimes for these bands cannot be calculated, being only possible for pure L-histidine where the intensity of the bands is much higher (see Table 2).

Discussion

The sample characterization in the Near Infrared region is relevant to data interpretation of missions like Mars 2020 and ExoMars. Indeed, the SuperCam infrared spectrometer on board the Mars 2020 Perseverance rover is currently analyzing rocks at Jezero crater in the 7692–3846 cm^{-1} spectral range[19–21]. In addition, the Ma_MISS and MicrOmega instruments on board the upcoming ExoMars Rosalind Franklin rover mission will work in the 25,000–4545 cm^{-1} and 10,526 – 2740 cm^{-1} spectral ranges, respectively[22,23]. As observed in the samples of L-histidine adsorbed onto nontronite (Table 1 and Figures S1A and S2A), this range exhibits few bands of the organic molecule, in particular at 6240 cm^{-1}, 5817 cm^{-1}, 4587 cm^{-1}, 4218 cm^{-1}, 3410 cm^{-1} and 2627 cm^{-1} in the case of the acidic sample and 6160 cm^{-1}, 4623 cm^{-1}, 4212 cm^{-1} and 2627 cm^{-1} in the case of the basic sample. It is important to notice that some of the bands in the NIR/MIR when L-histidine is adsorbed onto nontronite exhibit shifts in their position with respect to their original position on the pure amino acid, as

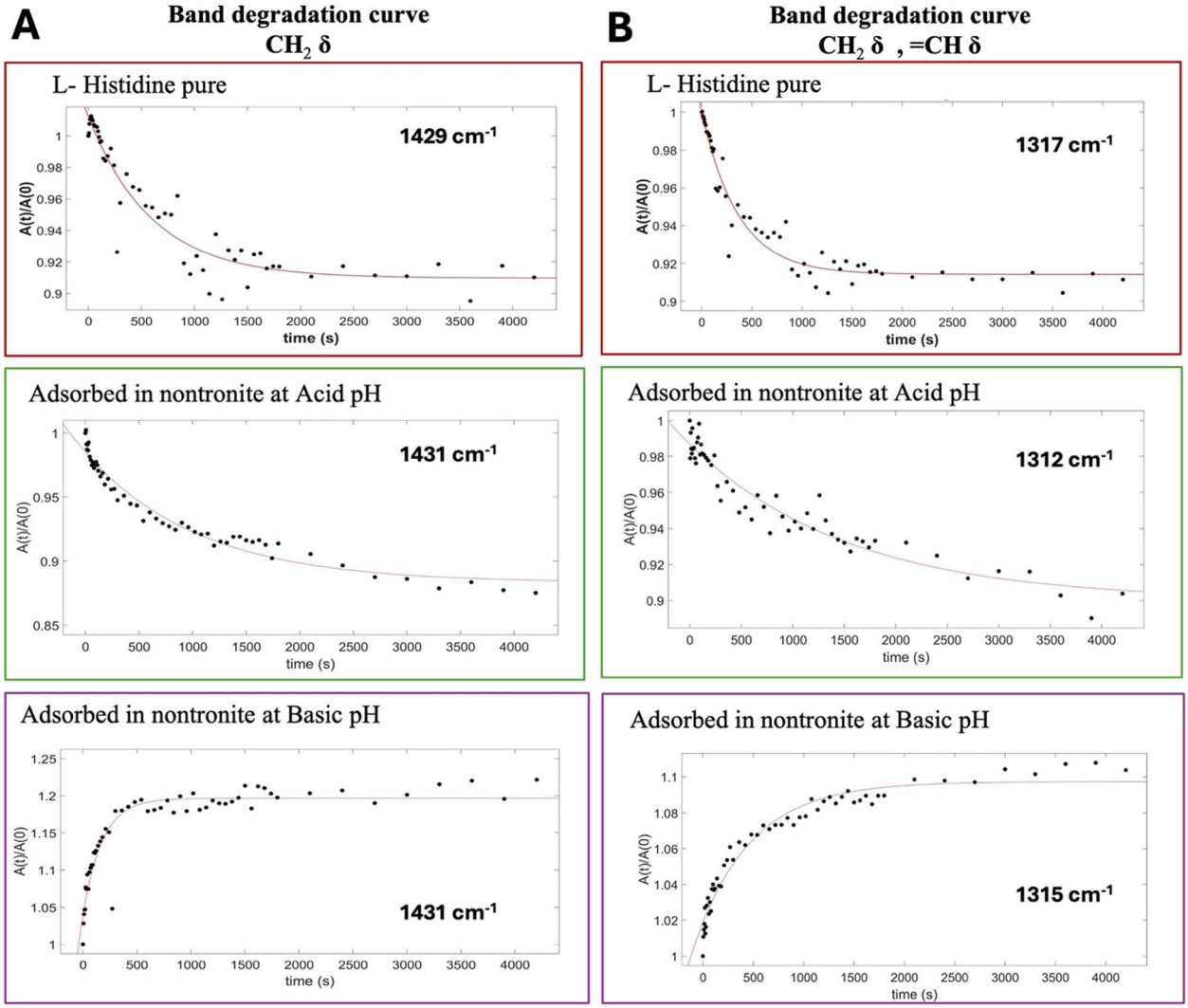

Fig. 5. Degradation curves for some of the bands assigned to the hydrocarbon part of the amino acid.

reported in Table 1 and Figures S1A and S2A. This can lead to an incorrect identification of the molecule on Mars if molecule-mineral interactions are not considered.

UV irradiation of the pure L-histidine shows a rapid degradation in the first 500–1000 s of irradiation and then degradation reaches a plateau after 2000–2500 s. A rapid initial degradation is also observed for the molecular bands of the samples adsorbed at acidic pH with a smoother trend as time passes. However, this degradation is always slower than the one observed for the pure molecule, while no degradation is observed at basic pH, as shown in Figs. 3, 4 and 5, S3 and S4. These different degradation rates may arise from the different molecule-mineral interactions.

Nontronite has a dioctahedral sheet with a 2:1 layer structure (TOT). Tetrahedral sheets (T) in nontronite are composed mainly of silicon (Si^{4+}), but occasional substitution with either Fe^{3+} or Al^{3+}, or combinations of these two cations can happen. This occasional substitution of Si^{4+} with Fe^{3+} gives to the nontronite an overall negative charged interlayer, which in the nontronite employed in this work is compensated with Na^{+} interlayer ions. The octahedral sheets are formed exclusively of Fe^{3+} (no aluminium was added during synthesis by Gainey et al. 2017>[32]) in this synthetic nontronite. Nontronite's basal surfaces (surfaces facing the interlayer) interact with adsorbates (such as water or cations) mostly through electrostatic interaction. The edge surfaces, instead, have amphoteric properties depending on the pH of the solution and can bind the organics through surface complexation[33]. The edges consist of O^{-}, OH and OH_2^{+} groups and their relative amounts depend on the pH of the aqueous environment at which the mineral is exposed[33]. At acidic pH, nontronite has positively charged edges, while at pH above 8, the edges are negatively charged[34]. On the other hand, L-histidine is positively charged at acidic pH (below 6), while it is negatively charged at basic pH (higher than 9).

Amino acids can be bound to minerals by cation exchange or complexation; positively charged amino acids can be adsorbed in the interlayer by cation exchange[17] and can interact through electrostatic interactions between the positively charged NH_3^{+} group and the negatively charged basal surfaces. This new interaction can cause a shift in the bands corresponding to the vibrational modes related to the NH_3^{+} functional group.

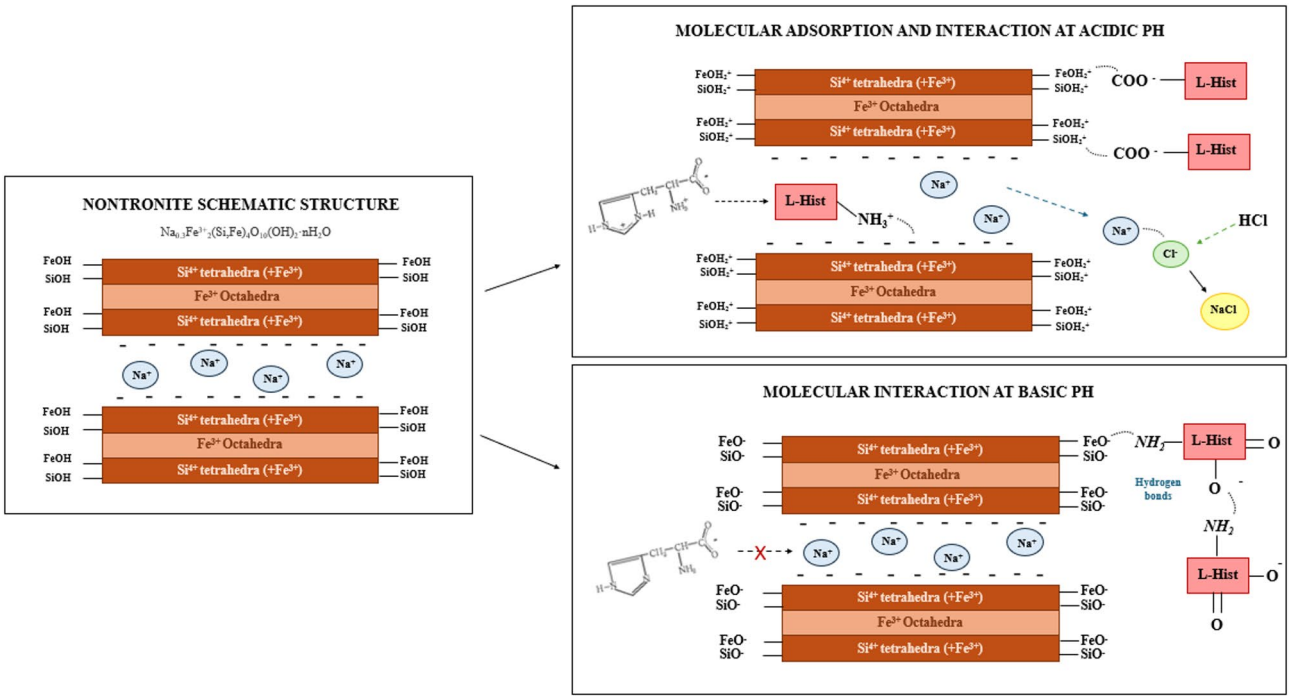

Fig. 6. Suggested interactions between L-histidine and nontronite at pH 4.6 and pH 9.8.

In this case, XRD analyses show an expansion of the interlayer when L-histidine is adsorbed at acidic pH in comparison to the pure mineral, suggesting that the molecule may be intercalated inside the interlayer of nontronite. This is corroborated by the shift observed in the IR spectrum for the band assigned to the NH_3^+ functional group probably due to the electrostatic interaction with the negatively charged interlayer (see Table 1 and Figure S1b). In addition, XRD shows the presence of NaCl that can be formed through the interactions of Cl^-, present in solution from the addition of HCl to achieve the desire acidic pH, and the Na^+ interlayer cations liberated in solution after cation exchange with the positively charged L-histidine inside the interlayer. The NaCl formation can also be detected in the nontronite blank at acidic pH likely due to a cation exchange between the Na^+ and the H^+ present due to the addition of the acid. This cation exchange does not produce a shift on the position of the *(001)* peak and the *hkl*-band (see Fig. 1) because it does not change the swelling state neither the structure of nontronite as the acid treatment was not too aggressive[35,36]. On the contrary, in the adsorption of L-histidine at acidic pH, a clear displacement of the *(001)* peak and *hkl*-band can be appreciated suggesting that the incorporation of additional molecules is causing the increase in the interlayer spacing.

In addition, in the IR spectrum, another shift of the bands related to COO^- suggests a second kind of interaction between the molecule and the mineral's positively charged OH_2^+ groups at the edges at acidic pH. In Fig. 6a schematic representation of the proposed interactions can be seen.

Overall, in the sample where L-histidine is adsorbed onto nontronite at acidic pH, the degradation of L-histidine while being exposed to UV-like Martian radiation is slower (higher half-life times) compared to the exposed pure molecule (see Table 2). This photoprotection probably arises from the mechanical shielding provided by nontronite to the intercalated molecule inside its interlayer.

At basic pH, the observed photoprotection cannot arise from the mechanical shielding as the negative charge prevents the molecule from the intercalation inside the interlayer. In the IR spectrum of the L-histidine adsorbed at basic pH, the shifts in some bands related to the NH and COO^- groups indicate two different interactions with the mineral. The edge groups of the external surface of the nontronite are negatively charged at pH 9.5 according to Zhang et al. 2009[34]. This means that the COO^- cannot interact directly with the mineral surface edge groups as in the adsorption at acidic pH. Based on the two observed shifts on IR and considering the negatively charge edge groups at basic pH, the only possible interaction is via hydrogen bond of polymolecular layers of L-histidine as previously observed by Kotova et al. 2022[37] in the adsorption of L-histidine onto other minerals. The first layer of L-histidine molecules may interact with the mineral surface edge groups via hydrogen bonds through the NH group giving rise to the observed shift in the bands related to this functional group in the IR spectrum. The second layer of molecules may be formed via a second hydrogen bond interaction between the COO^- groups of the molecules already adsorbed to the mineral surface and the NH group of the new second layer of molecules. This sequence may repeat forming polymolecular layers of L-histidine adsorbed onto nontronite at basic pH. In addition, the reduced crystallinity observed by XRD in the mineral with the molecule treated at basic pH may have been due to the effect of the high basic pH of the solution. However, the first diffraction peak in the XRD is not broader in the blank at basic pH indicating that the basifying process alone is not affecting the mineral structure. The loss of this crystallinity may arise, therefore, from the polymolecular adsorption mechanism of the molecule. The observation of no degradation of the bands of L-histidine when adsorbed on

nontronite at basic pH seems to suggest that the formation of these polymolecular layers of L-histidine makes the molecule more stable under UV radiation than the mechanical shielding offered by the mineral in the case of the molecule adsorbed in the interlayer when the adsorption occurs at acidic pH. In a layered assembly, amino acids arrange themselves optimizing intermolecular interactions such as hydrogen bonding that stabilize the system by reducing the overall energy providing a higher level of structural stability than what it is possible for an isolated molecule. The assembly we suggest based on the IR shifts and based on the capacity of single amino acids to form α-amine to α-carboxyl hydrogen bonds, generating chain-like or layered structures that resemble protein like aggregates, which are robust and stable[38].

Studies already reported in the literature show that the presence of Fe^{3+} in minerals may result in a high potential for organic preservation[17,39,40] due to its UV absorption capacity in opposite to Fe^{2+} that has been observed to photo-catalyse the degradation of organic molecules[40]. The UV absorption capacity of Fe^{3+} present in this nontronite may have play a key role in the photoprotection of L-histidine at acidic pH, by preventing the UV radiation to penetrate into the interlayer where the molecules are located. The UV absorption by Fe^{3+} might not be that important at basic pH where the polymolecular layers are formed at the surface of the mineral. A photoprotective effect of nontronite is also observed in the work by Poch et al., 2015[41], regarding two other amino acids, glycine and adenine. This work is also in agreement with the results of dos Santos et al., 2016[40] who analyzed the stability of several amino acids in different minerals, showing that nontronite had the highest preservation rate. However, another research, by Florentino et al. in 2025[18], studied the UV stability of L-histidine adsorbed on another clay mineral, saponite, at acidic and basic pHs. Their results, contrary to our results, indicate a photocatalytic behaviour of saponite due to the partial interaction of L-histidine with the surface edge sites of the mineral at both pHs, despite the potential shielding by interlayer sites for the part of L-histidine molecules intercalated in the interlayers at acidic pH[18].

Conclusions

This work shows that nontronite photoprotects L-histidine from UV irradiation both at acidic and basic pH. Mechanical shielding is responsible for the photoprotection when the molecule is adsorbed in the interlayer at acidic pH. Formation of polymolecular layers of L-histidine at basic pH appears to be even more effective. Such photoprotective properties make this mineral an appealing target to find organic molecules on Mars. Specifically, when L-histidine is adsorbed onto nontronite the half-life times calculated for the different functional groups are always superior to 1 sol, meaning that this molecule should still be detectable when the measurements by rover payload instruments can take place. In the case of Perseverance, for example, due to operational reasons, abraded patches of the rocks are exposed to ambient Martian UV for at least 1 sol before acquiring spectra with the SHERLOC spectrometer, which is the key instrument for organics detection. Thus, the detection of the organic molecules would only be possible if they remain photostable for at least 1 sol, which is the case of L-histidine adsorbed onto nontronite.

As observed also in a previous work of L-histidine adsorbed at different pHs in another smectite clay such as saponite[18], the different behaviour under UV depends on the interactions between the molecule and the mineral. Both these studies, therefore, indicate that molecule-mineral interactions represent the main factor affecting molecular stability under UV radiation. Since molecule-mineral interactions may vary depending on a variety of factors, it is very difficult to give general rules for best photoprotective minerals and therefore the study of other biomolecules such as glucose or fatty acids would be of interest.

In addition, this work shows that the detection of organics through NIR spectroscopy is very challenging when molecules are embedded into minerals, as most of the characteristic bands of the pure molecules can no longer be detected, even at much higher concentrations than the ones expected on Mars, and the few bands that are still detectable may present shifts with respect to the bands of the pure organic compound due to the interaction with the mineral. Moreover, the harsh Martian conditions due to high UV flux and presence of oxidants such as perchlorates[42] may alter the original organics and their spectroscopic features. Thus, for a proper interpretation of mission data and to correctly identify organic molecules on Mars, it is fundamental to assemble databases of spectroscopic features for molecule-mineral complexes under simulated Martian conditions.

Materials and methods

Synthesis of nontronite

Synthetic nontronite powder, synthesized in the laboratory after Gainey et al., 2017[32,43], following previous methods by Mizutani et al., 1991[44], was used as a mineral phase in the experiments[32]. Because it was synthesized in the laboratory under controlled conditions, it did not contain the organic matter expected to be present in natural nontronite. The nontronite was synthesized as follows. Briefly, 4.35 g of sodium metasilicate was dissolved in 420 ml of 18.2 MΩ water, and then acidified with 1.0 N H_2SO_4 to a pH of approximately 3. To maintain reducing conditions, all solutions were sparged with N_2, and then combined in the glove box with 4.2 g of sodium dithionite and 0.0142 mol of Fe(II)sulfate-heptahydrate. 19.8 mL of 5 M NaOH was added, which formed a precipitate that was then incubated in the glove box for one day. In the glove box, the suspension was then added to a Teflon-lined Parr vessel, which was then incubated at 150 °C for 4 days. The supernatant was then decanted from the clay mineral, and the clay mineral rinsed and centrifuged with spectrophotometric grade ethanol three times, and then air-dried under atmospheric conditions to allow oxidation of the ferrous iron to form nontronite[32].

Adsorption of l-histidine in nontronite

L-histidine was adsorbed onto nontronite at 10 wt% concentration to clearly detect molecular bands in the IR spectra and easily follow the degradation kinetics by observing changes in the molecular IR features during

UV irradiation. Specifically, 0.05 g of L-histidine (purity 99,5%, Sigma-Aldrich) was weighted and dissolved in 7mL of Milli-Q water. After complete solubilization, 0.5 g of nontronite were added. The desired pHs, acidic 4.6 and basic 9.8, were achieved by adding several drops of 2 M HCl or 1 M NaOH solutions, respectively, and were measured with the pHmeter Eutech pH 700. In addition, two blanks were prepared in the same way but without the addition of the molecule for both pHs to control any possible contamination and the effect of the process on the mineral itself. The acidic and basic suspensions were mixed with a vortex for 24 h in order to reach steady-state equilibrium[45] and maximise the interaction between the molecule and the mineral, favouring the establishment of physico-chemical interactions between the organic molecules and the mineral phase[45]. The pHs of the adsorption processes were monitored during the first hours in order to assure a pH < 6 at which the molecule has a total positive charged during the entire process for the acidic sample and pH > 9.6 to guarantee the negative charge of L-histidine for the basic sample. Both pHs were corrected when needed by adding some more HCl/NaOH drops. At the end of the 24 h adsorption processes, the pH was 4.6 for the acidic sample and 9.8 for the basic sample. At the end of the adsorption, the samples were transferred from the test-tubes to petri dishes to be dried at 30 °C in an oven.

IR spectroscopy and uv-radiation set up

Samples were characterized by Diffuse Reflectance InfraRed Fourier Transform Spectroscopy (DRIFTS) using a VERTEX 70v FT-IR spectrometer (Bruker) equipped with a Praying Mantis™ Diffuse Reflection Accessory (Harrick) which works in the spectral range from 8000 to 400 cm^{-1}, and the measurement was performed under a constant flux of nitrogen to avoid disturbances in the spectra bands from atmospheric CO_2 and H_2O. An infragold standard was taken under nitrogen flux before analysing the samples for the calibration of the instrument. The samples were measured using 200 scans for each spectrum with an instrumental resolution of 4 cm^{-1}.

The UV irradiation experiments were carried out using a Newport Oriel 300 W Xenon arc discharge lamp with a spectral range between 200 and 930 nm, interfaced with the Bruker VERTEX 70v interferometer. The UV light was focused directly on the sample through an optical fibre inserted into the IR sample compartment to monitor the infrared spectra in situ during the UV irradiation. All the surface of the sample, which presents an area of 7.07 mm^2 in the IR sample holder, was irradiated. The calculated UV flux arriving on the sample is of $\Phi_{Lamp} = 2.75 \cdot 10^{17}$ photons/s·cm^2 in the 200–400 nm spectral range as measured through a Spectro 320 monochromator scanning spectrometer[6]. The samples were put in the sample chamber and kept under a constant nitrogen flux during the entire experiment. The degradation of the molecule was monitored for a total time of 4200 s (1 h 10 min) by taking different Infrared spectra at certain steps. Specifically, infrared spectra were recorded initially every five seconds to monitor the quickest changes usually happening at the beginning of UV irradiation. Then, the time intervals between IR measurements were increased up to 5 min (300s). These total irradiations times were selected according to a previous work by García-Florentino et al.2025[18].

Data analyses

The evolution of L-histidine absorption bands upon UV irradiation was quantified using MATLAB (R2024a). Only bands not overlapping with nontronite features were considered and analyzed individually. For each selected band, spectra were first cropped within a user-defined wavenumber range. The baseline was then approximated by a linear interpolation between the two edges of the selected band and removed by division, in order to account for slope variations in reflectance. To facilitate quantitative comparison, the corrected spectra were transformed by subtracting the baseline (i.e., 1 – corrected signal), effectively setting the continuum to zero and converting absorption features into positive peaks (e.g., see Fig. 2). The integrated band area was then calculated using the trapezoidal numerical integration method (trapz function in MATLAB). For assessing the degradation of the bands, areas were normalized to the initial (pre-irradiation) value, enabling the comparison of degradation trends over time.

The data were then fitted to a first-order kinetics Eq. 1:

$$\frac{A(t)}{A(0)} = Be^{-\beta t} + C \tag{1}$$

where A(t) is the area of the infrared band at irradiation time t, proportional to the number of molecules at that time, $A(0)$ is the area of the band before the irradiation process, proportional to the initial number of molecules, B is the fraction of molecules that interact with UV radiation, β is the degradation rate and C is the fraction of molecules that do not interact with UV radiation flux.

The half-lifetimes ($t_{1/2}$) of degradation for each detectable band were calculated according to the Eq. 2:

$$t_{\frac{1}{2}} = \frac{\ln 2}{\beta} \tag{2}$$

The UV destruction cross section σ were then calculated according to the Eq. 3:

$$\sigma = \frac{\beta}{\varphi_{LAMP}} \tag{3}$$

The degradation cross section is a characteristic parameter of the molecule, which does not change and therefore it can be used to make an extrapolation and approximate a degradation rate for each band on Mars with the Martian UV flux. To estimate the survivability of the L-histidine on Mars, the Martian UV flux value of

$\Phi_{\text{MarsPatel}} = 1.4 \cdot 10^{15}$ photons $\cdot\, s^{-1} \cdot cm^{-2}$ (in the 190 – 325nm spectral region, assuming dust free atmosphere at the noontime equator) as estimated by Patel et al. 2002[46] was used.

X-ray diffraction characterization

The powder samples were characterized in boron-silicate glass capillaries of 0.3 mm X-ray diffraction in air, performed at the ESD-MI with a Rigaku XtaLAB Synergy-S diffractometer equipped with a HyPix-6000HE detector and a PhotonJet-S Mo-Kα (λ = 0.71075 Å) microsource, operating at 50 kV and 1 mA. X-ray diffraction data were collected with an omega step size of 0.5° and 40 s per step of exposure time. Qualitative analysis of the XRD pattern was performed with X'Pert High Score software. The coherent domain size values were determined using the GSAS-II software package through Rietveld refinement[47,48]. More specifically, they were obtained from the analysis of the XRD peak profiles after correcting for instrumental broadening.

Data availability

The datasets used and/or analysed during the current study available from the corresponding author on reasonable request.

Received: 30 January 2026; Accepted: 5 May 2026
Published online: 18 May 2026

References

1. Khan, A. et al. Evidence for a liquid silicate layer atop the Martian core. *Nature* **622**, 718–723 (2023).
2. Samuel, H. et al. Geophysical evidence for an enriched molten silicate layer above Mars's core. *Nature* **622**, 712–717 (2023).
3. Arvidson, R. E. et al. Ancient aqueous environments at Endeavour crater. *Mars Sci.* **343**, 1248097 (2014).
4. Fornaro, T., Steele, A. & Brucato, J. R. Catalytic/protective properties of Martian minerals and implications for possible origin of life on Mars. *Life* **8**, 56 (2018).
5. Grotzinger, J. P. et al. A habitable fluvio-lacustrine environment at Yellowknife Bay, Gale crater. *Mars Sci.* **343**, 1242777 (2014).
6. Alberini, A. et al. Investigating the stability of aromatic carboxylic acids in hydrated magnesium sulfate under UV irradiation to assist detection of organics on Mars. *Sci. Rep.* **14**, 15945 (2024).
7. Connell, S. A. et al. Abrasion patch dehydration experiment at Bright Angel, Jezero Crater, using SuperCam onboard the Mars 2020 Perseverance Rover. *J. Geophys. Res. Planets* **130**, e2025JE009243 (2025).
8. Alberini, A. et al. Photostability of polycyclic aromatic hydrocarbons in hydrated magnesium sulfate under Martian ultraviolet irradiation to assist organics detection on Mars. *Sci. Rep.* **15**, 40484 (2025).
9. Fornaro, T. et al. Evidence for polycyclic aromatic hydrocarbons detected in sulfates at Jezero crater by the Perseverance rover. *Nat. Astron.* **9**, 1648–1661 (2025).
10. Hurowitz, J. A. et al. Redox-driven mineral and organic associations in Jezero Crater. *Mars Nat.* **645**, 332–340 (2025).
11. Millan, M. et al. Sedimentary organics in Glen Torridon, Gale Crater, Mars: Results from the SAM instrument suite and supporting laboratory analyses. *J. Geophys. Res. Planets* **127**, e2021JE007107 (2022).
12. Eigenbrode, J. L. et al. Organic matter preserved in 3-billion-year-old mudstones at Gale crater. *Mars Sci.* **360**, 1096–1101 (2018).
13. Freissinet, C. et al. Long-chain alkanes preserved in a Martian mudstone. *Proc. Natl. Acad. Sci. U. S. A.* **122**, e2420580122 (2025).
14. Carter, J., Poulet, F., Bibring, J.-P., Mangold, N. & Murchie, S. Hydrous minerals on Mars as seen by the CRISM and OMEGA imaging spectrometers: Updated global view. *J. Geophys. Res. Planets* **118**, 831–858 (2013).
15. Milliken, R. E., Grotzinger, J. P. & Thomson, B. J. Paleoclimate of Mars as captured by the stratigraphic record in Gale Crater. *Geophys. Res. Lett.* https://doi.org/10.1029/2009GL041870 (2010).
16. Brossier, J. et al. Constraining the spectral behavior of the clay-bearing outcrops in Oxia Planum, the landing site for ExoMars "Rosalind Franklin" rover. *Icarus* **386**, 115114 (2022).
17. Gil-Lozano, C. et al. Constraining the preservation of organic compounds in Mars analog nontronites after exposure to acid and alkaline fluids. *Sci. Rep.* **10**, 15097 (2020).
18. García-Florentino, C. et al. Photodegradation of the biomarker L-histidine induced by edge sites of a clay mineral in the Martian harsh UV environment. *Icarus* **442**, 116757 (2025).
19. Wiens, R. C., Maurice, S. & Perez, F. R. The SuperCam remote sensing instrument suite for the Mars 2020 rover: A preview. *Spectroscopy (Santa Monica)* **32**, 50–55 (2017).
20. Wiens, R. C. et al. The SuperCam Instrument Suite on the NASA Mars 2020 Rover: Body Unit and Combined System Tests. *Space Sci. Rev.* **217**, 4 (2020).
21. Maurice, S. et al. The SuperCam Instrument Suite on the Mars 2020 Rover: Science Objectives and Mast-Unit Description. *Space Sci. Rev.* **217**, 47 (2021).
22. Bibring, J.-P., Hamm, V., Pilorget, C. & Vago, J. L. The MicrOmega Investigation onboard ExoMars. *Astrobiology* **17**, 621–626 (2017).
23. De Sanctis, M. C. et al. Ma_MISS on ExoMars: Mineralogical Characterization of the Martian Subsurface. *Astrobiology* **17**, 612–620 (2017).
24. Brown, G. & Brindley, G. W. X-ray Diffraction Procedures for Clay Mineral Identification. in Crystal Structures of Clay Minerals and their X-Ray Identification (eds Brindley, G. W. & Brown, G.) (5 0 (Mineralogical Society of Great Britain and Ireland, (1980).
25. Frost, R. L., Kloprogge, J. T. & Ding, Z. Near-infrared spectroscopic study of nontronites and ferruginous smectite. *Spectrochim. Acta A Mol. Biomol. Spectrosc.* **58**, 1657–1668 (2002).
26. Gonsago, C. A., Albert, H. M., Malliga, P. & Arul Pragasam, A. J. Growth and characterization of pure and thiourea doped L-Histidine single crystals. *Mater. Manuf. Process.* **27**, 355–359 (2012).
27. Kumar, S., Rai, A. K., Rai, S. B. & Rai, D. K. Infrared and Raman spectra of Histidine: An ab initio DFT calculations of Histidine molecule and its different protonated forms. *Indian J. Phys.* **84**, 563–573 (2010).
28. Mesu, J. G., Visser, T., Soulimani, F. & Weckhuysen, B. M. Infrared and Raman spectroscopic study of pH-induced structural changes of l-Histidine in aqueous environment. *Vib. Spectrosc.* **39**, 114–125 (2005).
29. Deplazes, E. et al. A combined theoretical and experimental study of the structure and vibrational absorption, vibrational circular dichroism, Raman and Raman optical activity spectra of the L-histidine zwitterion. *Theor. Chem. Acc.* **119**, 155–176 (2008).
30. Deacon, G. B. & Phillips, R. J. Relationships between the carbon-oxygen stretching frequencies of carboxylato complexes and the type of carboxylate coordination. *Coord. Chem. Rev.* **33**, 227–250 (1980).
31. Dammak, T. et al. Structural, vibrational and ab initio studies of l-Histidine oxalate. *Spectrochim. Acta A Mol. Biomol. Spectrosc.* **66**, 1097–1101 (2007).
32. Gainey, S. R. et al. Clay mineral formation under oxidized conditions and implications for paleoenvironments and organic preservation on Mars. *Nat. Commun.* **8**, 1230 (2017).

33. Gao, P., Liu, X., Guo, Z. & Tournassat, C. Acid-base properties of cis-vacant Montmorillonite edge surfaces: A combined first-principles molecular dynamics and surface complexation modeling approach. *Environ. Sci. Technol.* **57**, 1342–1352 (2023).
34. Zhang, G. et al. Microbial reduction of iron(III)-rich nontronite and uranium(VI). *Geochim. Cosmochim. Acta* **73**, 3523–3538 (2009).
35. Ramirez, S., Righi, D. & Petit, S. Alteration of smectites induced by hydrolytic exchange. *Clay Miner.* **40**, 15–24 (2005).
36. Angaji, M. T., Zinali, A. Z. & Qazvini, N. T. Study of physical, chemical and morphological alterations of smectite clay upon activation and functionalization via the acid treatment. *World J. Nano Sci. Eng.* **3**, 161–168 (2013).
37. Kotova, D. L., Krysanova, T. A., Novikova, L. A., Belchinskaya, L. I. & Petukhova, G. A. Exchange and nonexchange interactions during the sorption of histidine on clinoptilolite and glauconite. *Prot. Met. Phys. Chem. Surf.* **58**, 282–286 (2022).
38. Bera, S., Mondal, S., Rencus-Lazar, S. & Gazit, E. Organization of amino acids into layered supramolecular secondary structures. *Acc. Chem. Res.* **51**, 2187–2197 (2018).
39. Bishop, J. L., Louris, S. K., Rogoff, D. A. & Rothschild, L. J. Nanophase iron oxides as a key ultraviolet sunscreen for ancient photosynthetic microbes. *Int. J. Astrobiol.* **5**, 1–12 (2006).
40. dos Santos, R., Patel, M., Cuadros, J. & Martins, Z. Influence of mineralogy on the preservation of amino acids under simulated Mars conditions. *Icarus* **277**, 342–353 (2016).
41. Poch, O. et al. Effect of nontronite smectite clay on the chemical evolution of several organic molecules under simulated Martian surface ultraviolet radiation conditions. *Astrobiology* **15**, 221–237 (2015).
42. Glavin, D. P. et al. Evidence for perchlorates and the origin of chlorinated hydrocarbons detected by SAM at the Rocknest Aeolian Deposit in Gale Crater. *J. Geophys. Res. Planets* **118**(10), 1955–1973. https://doi.org/10.1002/jgre.20144 (2013).
43. Harrold, Z. R. et al. Bioavailability of mineral-bound iron to a snow algal-bacterial coculture and implications for albedo-altering snow algal blooms. *Appl. Environ. Microbiol.* **84**, e02322-17 (2018).
44. Mizutani, T. Synthesis of 1:1 and 2:1 iron phyllosilicates and characterization of their iron state by Mössbauer spectroscopy. *Clays Clay Miner.* **39**, 381–386 (1991).
45. Fornaro, T. et al. UV irradiation and near infrared characterization of laboratory Mars soil analog samples. *Front. Astron. Space Sci.* https://doi.org/10.3389/fspas.2020.539289 (2020).
46. Patel, M. R., Zarnecki, J. C. & Catling, D. C. Ultraviolet radiation on the surface of Mars and the Beagle 2 UV sensor. *Planet. Space Sci.* **50**, 915–927 (2002).
47. Rietveld, H. M. The Rietveld method. *Phys. Scr.* **89**, 98002. https://doi.org/10.1088/0031-8949/89/9/098002 (2014).
48. Toby, B. H. & Von Dreele, R. B. GSAS-II : The genesis of a modern open-source all purpose crystallography software package. *J. Appl. Crystallogr.* **46**, 544–549. https://doi.org/10.1107/S0021889813003531 (2013).

Acknowledgements

This research was supported by the Italian Space Agency (ASI) through the ASI/INAF agreement n. 2023-3-HH. This work was also supported by INAF through the Large Grant 2024 "Laboratory investigations to assess the astrobiological relevance of the Martian samples collected on Mars by the NASA Mars 2020 Perseverance rover for the future return to Earth".

Author contributions

C.G.F: conceptualization,methodology, formal analysis, investigation, writing original-draft, visualization. I.B: conceptualization, methodology, analysis, investigation, writing original manuscript, visualization. T.F: conceptualization, methodology, resources, writing original manuscript, writing review and editing, supervision, project administration, funding acquisitionA.A: conceptualization, methodology, software, data curation, writing review N.M: analysis, investigation, writing original manuscriptM.M: analysis, investigationS.B: methodology, writing review F.R: methodology, writing review G.P: methodology, writing reviewM.B: writing review E.M.H: Resources acquisition, writing original manuscriptJ.R.B: conceptualization, methodology, resources, writing review and editing, supervision, project administration, funding acquisition.

Funding

This research was supported by the Italian Space Agency (ASI) through the ASI/INAF agreement n. 2023-3-HH. This work was also supported by INAF through the Large Grant 2024 "Laboratory investigations to assess the astrobiological relevance of the Martian samples collected on Mars by the NASA Mars 2020 Perseverance rover for the future return to Earth".

Declarations

Competing interests

The authors declare no competing interests.

Additional information

Supplementary Information The online version contains supplementary material available at https://doi.org/10.1038/s41598-026-52355-4.

Correspondence and requests for materials should be addressed to C.G.-F. or I.B.

Reprints and permissions information is available at www.nature.com/reprints.

Publisher's note Springer Nature remains neutral with regard to jurisdictional claims in published maps and institutional affiliations.

Open Access This article is licensed under a Creative Commons Attribution-NonCommercial-NoDerivatives 4.0 International License, which permits any non-commercial use, sharing, distribution and reproduction in any medium or format, as long as you give appropriate credit to the original author(s) and the source, provide a link to the Creative Commons licence, and indicate if you modified the licensed material. You do not have permission under this licence to share adapted material derived from this article or parts of it. The images or other third party material in this article are included in the article's Creative Commons licence, unless indicated otherwise in a credit line to the material. If material is not included in the article's Creative Commons licence and your intended use is not permitted by statutory regulation or exceeds the permitted use, you will need to obtain permission directly from the copyright holder. To view a copy of this licence, visit http://creativecommons.org/licenses/by-nc-nd/4.0/.

© The Author(s) 2026